Molecular structural effects in below- and near-threshold harmonics in XUV-comb generation

MuFeng Zhu,[1,2] Jin Zhang,[1,2] LinQiang Hua,[1,*] ZhengRong Xiao,[1,2] SongPo Xu,[1] XuanYang Lai,[1] and XiaoJun Liu[1,†]

[1]*State Key Laboratory of Magnetic Resonance and Atomic and Molecular Physics, Innovation Academy for Precision Measurement Science and Technology, Chinese Academy of Sciences, Wuhan 430071, China*

[2]*University of Chinese Academy of Sciences, Beijing 100049, China*

(Received 16 August 2021; revised 1 October 2021; accepted 5 October 2021; published 25 October 2021)

The below- and near-threshold harmonics generated by O_2 molecules and Xe atoms have been investigated experimentally by using an extreme-ultraviolet (XUV)-comb setup that is driven by an intense 1040-nm laser field. It is found that the yields of the below- and near-threshold harmonics generated by O_2 molecules show a significant suppression when compared to Xe, although the two species have nearly identical ionization potentials. Our theoretical analysis shows that the harmonic yield suppression is related to the two-center interference effect of O_2 and the tightly bounded orbital of the O atom. Our study provides useful information for the XUV-comb technique when extending the working media from atoms to complex systems.

DOI: 10.1103/PhysRevA.104.043111

I. INTRODUCTION

The extreme-ultraviolet (XUV) comb is a powerful tool which has already demonstrated many applications and offered new opportunities in the fields of precision spectroscopy and ultrafast science [1]. For example, direct XUV frequency-comb spectroscopy [2] has the potential to measure the atomic transitions in the XUV region, such as the $1S$-$2S$ transition of He at 120 nm [3,4], He^+ at 61 nm [5,6], or Li^+ at 40.7 nm [7]. These transitions provide the possibilities of stringent tests on the quantum electrodynamics theory [6] and measurements of the subtle variation of the fine-structure constant [8]. On the other hand, a nuclear transition in the ^{229}Th ion driven by an XUV frequency comb gives a promising candidate of an optical clock with an extraordinary stability [8–12]. In the ultrafast realm, the high-repetition-rate XUV-frequency-comb setup promotes time-resolved studies of dynamics in molecular and solid-state systems on femtosecond and even attosecond timescales [13–15].

A well-accepted way to generate the XUV comb is through a nonlinear frequency conversion process, i.e., high-order harmonic generation (HHG) [16,17], within the femtosecond enhancement cavity (fsEC) [16–19]. HHG spectra have structural characteristics as follows. In the very beginning, the harmonic yield drops exponentially with the increase of the harmonic order due to the decreasing nonlinear susceptibility [20]. Then, after the fast drop in the yields of the first few orders, the HHG spectrum shows a long plateau, where the harmonic yield changes little with the increase of the harmonic order. Finally, this plateau is followed by a sharp cutoff with the increase of the photon energy [21]. The generation process for the harmonics above the atomic ionization potential I_p can be well understood by the semiclassical three-step model [22,23]. First, an electron is liberated from the parent nucleus by the action of a driving field, and then it oscillates quasifreely in the laser field and acquires additional kinetic energy. And finally, it may have a small chance to return to the parent ion and emit harmonic radiations. In the past few decades, most strong-field studies of HHG have focused on the above-threshold harmonic region (photon energy above I_p). However, with the invention of the vacuum-ultraviolet and extreme-ultraviolet frequency combs, study of the below- or near-threshold harmonics becomes more and more important [24], not only because the below- or near-threshold harmonics are usually located before the plateau region, and thus the conversion efficiency is relatively high, but also because these harmonics can help us to understand the complex ionization mechanism of tunnel ionization and multiphoton ionization [25,26] and shed light on the electron dynamics of the bound electron [27–29]. For example, an XUV comb with a generated power of ∼2 mW using near-threshold harmonics at the 11th order, i.e., ∼97 nm, has been achieved with a He:Xe gas mixture [30]. This is so far the highest generated power reported for a comb in the XUV region. On the other hand, Yost *et al.* [24] observed the quantum path interference within the below- or near-threshold harmonics, and the two dominant paths could be designated as the short trajectories and the long trajectories. The short trajectories indicate a multiphoton excitation and recombination process while the long trajectories can be described by the inclusion of the Coulomb potential in the simple man's model.

Recently, researchers have extended the XUV-comb technology from atomic HHG to molecular HHG [13,31]. By using the aligned N_2O molecule, Benko *et al.* [13] found that the XUV-comb yields with aligned molecules show a nearly 50% enhancement compared with the yields with unaligned molecules. Meanwhile, they investigated the modulation of the molecular alignment effect on the phase of the XUV frequency comb. Later, Zhang *et al.* observed an obvious spectral broadening of the driving field [31] when O_2 was used as

*hualq@wipm.ac.cn
†xjliu@wipm.ac.cn

the interaction media in the fsEC during the HHG process. This spectral broadening was due to the impulsive stimulated Raman excitation of the rotational states of O_2. These studies show that molecules provide additional degrees of freedom to be manipulated compared to atoms, and controlling over some of these parameters can be beneficial to XUV-comb-related studies and even XUV-comb generation itself (e.g., oriented molecules can be used to generate even-order harmonics [32] and thus have the potential to broaden the spectra of the current XUV-comb setup). On the other hand, these studies also raise the question of how molecular effects, such as the structural effect, affect the detailed dynamics of XUV comb generation. Although molecular HHG have been studied extensively [33–42] and some physical effects relevant to the molecular structure, such as the two-center interference effect, on the harmonic yields in the plateau region have been observed [40,41], how the structural effects manipulate the dynamics of the below- and near-threshold harmonics, which are important in XUV-comb generation and control, have not been addressed yet.

In this paper, we perform a comparison study of the below- and near-threshold harmonics that are generated by O_2 molecules and Xe atoms by using an XUV-comb setup. We find that those harmonics generated by O_2 show a significant suppression, not only in the plateau region but also in the below- and near-threshold harmonics. We theoretically reproduce the experimental results and analyze the underlying physical mechanism by using a modified semiclassical method. In this method, the atomic potential is included in both the initial ionization processes and the subsequent continuum dynamics, so that part of the below- or near-threshold harmonic generation process can be understood in terms of semiclassical dynamics. Our analysis shows that the suppression of the below- or near- threshold harmonic yield of O_2 compared to that of Xe could be attributed to the different structures of them. The destructive interference effect from the two atomic centers of O_2, together with the different atomic orbital effect, accounts for the peculiar suppression of the below- or near-threshold harmonic yield of O_2.

This paper is organized as follows. In Sec. II, we show our experimental setup, and in Sec. III, we give a brief description of our theoretical model, i.e., the modified semiclassical method. Then in Sec. IV, we discuss the experimental results and the theoretical interpretations. Finally, in Sec. V our conclusions are given.

II. EXPERIMENTAL SETUP

As schematically shown in Fig. 1, our experiment employs a 100-MHz repetition rate Yb-doped fiber frequency comb (Active Fiber systems) with a maximum output pulse energy of 1 μJ, spectrally centered at 1040 nm, to coherently seed a fsEC. The pump laser could be enhanced by tens or hundreds of times in the fsEC, and the details of our fsEC have been described in Refs. [31,43,44]. When the pump power is 24 W, an average power of 4.5 kW can be obtained inside the cavity, and the corresponding buildup is 188. The pulse duration is measured to be ~330 fs by a frequency-resolved optical gating. With a focus radius of 8 μm (vertical) × 16 μm (horizontal), a peak intensity of 3.3×10^{13} W/cm^2 is

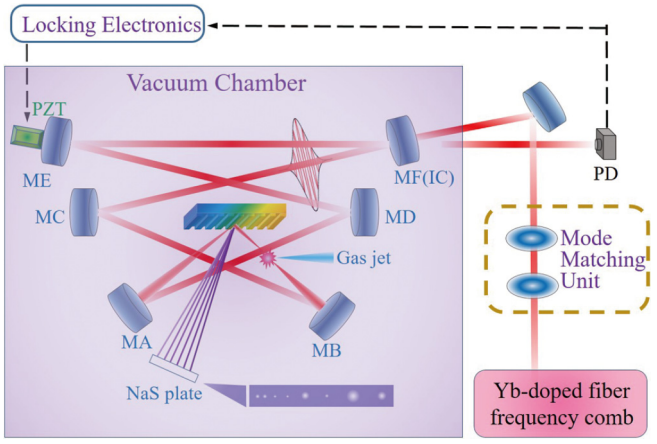

FIG. 1. Schematic view of our experimental setup. PZT, piezo transducer; IC, input coupler; PD, photodiode; NaS plate, sodium salicylate plate; MA–MF, mirror A to mirror F.

reached at the focus. A quartz gas nozzle with a diameter of 150 μm, positioned near the cavity focus, is used to inject the gas medium (pure Xe or O_2) into the cavity. It is installed on a three-dimensional translation stage with the aim to precisely optimize the harmonic signal. After interacting with the gas, the beam impinges on the grating mirror (GM) under a 70° grazing-incidence angle. The GM is a multilayer dielectric stack mirror with a diffraction nanograting (a period of 420 nm, a step height of 40 nm, and a duty cycle of 40%) etched on the top layer. With this design, the GM could couple the harmonics out of the cavity and maintain the high reflectivity for the fundamental light. A sodium salicylate plate is used to image the profiles of the harmonics that are out coupled from the cavity.

III. THEORETICAL METHODS

In order to understand the below- and near-threshold harmonics observed in the experiment, we develop a modified semiclassical theoretical model, based on the generalized semiclassical model [26] and the Lewenstein model [45]. In the generalized semiclassical model [26,46], the amplitude of the qth harmonic is written as the superposition of the contributions of different kinds of quantum orbits,

$$T_q \sim \sum_j a_j \exp\left(iS_q^j\right), \tag{1}$$

where a_j and S_q^j represent the amplitude and the phase of the jth trajectory, respectively. For convenience, we consider a one-dimensional model, and specifically, the phase S_q^j is given by

$$S_q^j = -\frac{1}{2}\int_{t_{0j}}^{t_{rj}} \left\{\frac{[v(t')]}{2} - E(t')x(t') - V(x)\right\}dt' - I_p(t_{rj} - t_{0j}) + q\omega t_{rj}, \tag{2}$$

where $V(x)$ is the Coulomb potential, I_p is the ionization potential, $E(t)$ is the electric field of the laser pulse, and t_{0j} and t_{rj} are the ionization time and the return time of the jth trajectory, respectively. In our work, the Coulomb potential of

the Xe atom is given by [26]

$$V_a(x) = -\frac{1}{\sqrt{x^2 + \left(\frac{1}{U_0}\right)^2}}, \tag{3}$$

with $U_0 = 0.063$, and the Coulomb potential of O_2 is [47]

$$V(x) = -\sum_{i=1}^{2} \frac{Z_\infty + (Z_0 - Z_\infty)\exp\left(-\frac{|x-R_i|^2}{b^2}\right)}{\sqrt{|x-R_i|^2 + a^2}}, \tag{4}$$

where R_i represents the position of each atomic center and $Z_\infty = 0.5$, $a = 1.0$, and $b = 0.771$ to match the ionizing energy of the $1\pi_g$ orbital of O_2. The quantum orbits are obtained by solving the Newton equations of motion, with the initial position $x(t_0) = \frac{I_p + \sqrt{I_p^2 - 4|E(t_0)|}}{2|E(t_0)|}$ and the initial velocity $v(t_0) = 0$ [26]. In practice, we vary the tunneling time t_0 to obtain a large number of trajectories. Those trajectories with the return energy of $q\omega$ correspond to the generation of the qth harmonic. Our result shows that, for each harmonic, there are usually two trajectories with travel time less than 1.1 optical cycles. Other trajectories with longer travel time are neglected in our simulation due to the propagation effect. In addition, to compare with the measurement, a monochromatic laser electric field of $E(t) = E_0\cos(\omega t)$ is used in our simulation and we assume that the harmonic emission is the same in each optical cycle, which is different from the calculation of the HHG with a few-cycle laser pulse [48].

In order to consider the quantum effect during the tunneling ionization and the recombination processes, we modify the generalized semiclassical model by considering the complex tunneling time and the complex return time based on the Lewenstein model [45,49]. In the Lewenstein model [45], the complex tunneling time $t_0 + it_{0i}$ satisfies the following conditions [49]:

$$[p_0 + A(t_0 + it_{0i})]^2 = -2I_p, \tag{5a}$$

$$p_0 + A(t_0) = v_0. \tag{5b}$$

The first equation denotes the energy conservation during the tunneling, and the second one is the velocity at the tunneling exit. After solving these two equations, we can obtain the imaginary part of the tunneling time t_{0i}. Similarly, for the recombination process, the imaginary part of the return time t_{ri} is obtained by solving the following equations:

$$[p_r + A(t_r + it_{ri})]^2 = 2(q\omega - I_p), \tag{6a}$$

$$p_r + A(t_r) = v_r. \tag{6b}$$

The first equation also denotes the energy conservation during the photoemission and the second one is the return velocity of the electron at the real time t_r. By using the complex tunneling time and the complex return time, the second and third terms on the right-hand side of Eq. (2) are updated in our theoretical method.

On the other hand, the intensity a_j in Eq. (1) is given by [45]

$$a_j = d_{\rm ion}(\tilde{p}(t_{0j}))d^*_{\rm rec}(\tilde{p}(t_{rj})), \tag{7}$$

where $j = 1$ and 2, $d_{\rm ion}(\tilde{p}(t_0)) = \langle\tilde{p}(t_0)|H_{\rm int}(t_0)|\psi_0\rangle$ denotes the ionization of the electron from a field-free bound state $|\psi_0\rangle$ to a Volkov state $|\tilde{p}(t_0)\rangle$, and $d_{\rm rec}(\tilde{p}(t_r)) = \langle\tilde{p}(t_r)|x|\psi_0\rangle$ represents the recombination of the ionized electron. In the velocity gauge, $\tilde{p}(t) = p$ and $H_{\rm int}(t_0) = [p_0 + A(t)]^2/2$ [50], where p is the canonical momentum of the electron at the time t. In this work, the initial bound states ψ_0 of Xe and O_2 are written as the linear combination of atomic orbitals [42,51–53] and the corresponding coefficients are extracted from the GAUSSIAN 09 quantum chemistry code [54].

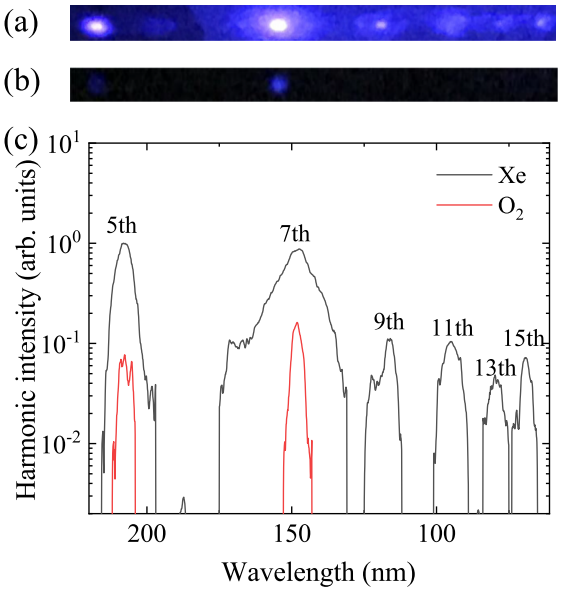

FIG. 2. Image of the experimentally observed high-order harmonics fluorescing on a sodium salicylate plate of (a) Xe and (b) O_2, respectively. The intensity of the laser field is about 3.3×10^{13} W/cm^2. (c) The spectra of the out coupled high-order harmonic radiation of Xe and O_2 obtained from the images of the fluorescent plate. The order of each harmonic is also marked.

IV. RESULTS AND DISCUSSIONS

In Fig. 2(a), we show the recorded image of the HHG on the fluorescent plate for Xe. The intensity of the laser field is estimated to be 3.3×10^{13} W/cm^2. The background pressure is set to be ~0.1 atm to avoid power fluctuation in the fsEC [2] that is induced by steady-state plasma [30,55]. The discrete spots on the fluorescent screen represent different harmonic orders and harmonics from the 5th to the 15th can be directly observed on the fluorescent plate under the current experimental conditions. We perform the same measurement for O_2 under identical experimental conditions. However, we find that the harmonic signal is rather weak and it is hard to observe with a camera. Thus, we increase its background pressure to ~0.5 atm and the results are shown in Fig. 2(b). The 5th and 7th harmonics can be directly observed while others are still beyond the detection threshold of the fluorescent plate. We integrate each two-dimensional image along the vertical direction to obtain a one-dimensional spectrum. After wavelength calibration, we can obtain the harmonic spectra of Xe and O_2 and they are shown in Fig. 2(c). It is clear that the harmonic yields of the 5th to 15th orders for O_2 all show a significant suppression compared to that of Xe. It is noteworthy that the ionization energies of Xe and O_2 are 12.13 and 12.07 eV,

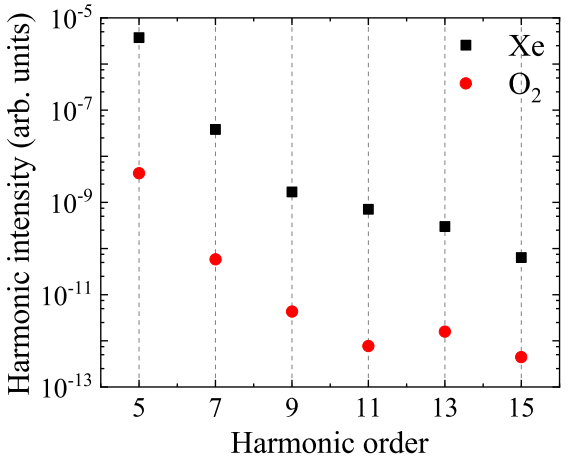

FIG. 3. Harmonic yields as a function of harmonic order for Xe and O_2, respectively, calculated with the modified semiclassical method. The laser wavelength is 1040 nm and the peak intensity is 3.3×10^{13} W/cm^2. For comparison with the experimental result, the alignment average of the molecular axis is considered in our simulation.

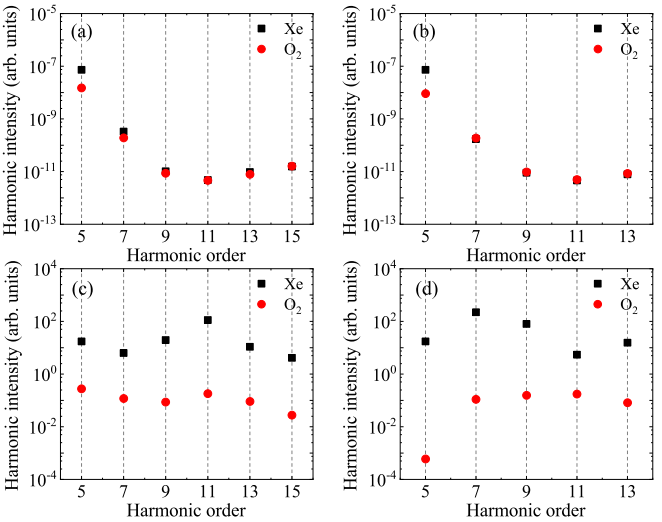

FIG. 4. Absolute value of $\exp(iS_q^j)$ and a_j of each trajectory for O_2 and Xe, respectively. Panels (a) and (b) are for $\exp(iS_q^j)$; panels (c) and (d) are for a_j. The left column is for the first trajectory; the right column is for the second trajectory.

respectively, which coincide with 10.1 and 10.2 harmonic order. Therefore, our experimental results indicate that the suppression of harmonic yield not only exists in the plateau region but also appears in the below- and near-threshold harmonic regions. The suppression of harmonic yield in the plateau region has been studied by several groups [53,56,57] and has been well understood by the two-atomic-center interference effect on strong-field tunnel ionization of the O_2 molecule in the frame of the Ammosov-Delone-Krainov model and the Lewenstein model [56–58]. However, because the underlying physics for the near- and below-threshold harmonics is still unclear, less attention has been paid to this energy region. In this paper, the suppression of the near - and below - threshold harmonic yields are reported and the underlying physics are revealed with our modified semiclassical method.

In order to explore the underlying mechanisms for the suppression of the below- and near-threshold harmonic yields of O_2 compared to that of Xe, we simulate the HHG spectra by using our modified semiclassical method. In our experiment, O_2 molecules are randomly oriented. Thus, we calculate all the molecular alignment angles from 0° to 180° and then take the average results in the simulation for a better comparison. Figure 3 shows the simulated HHG spectra of Xe and O_2 using the same laser parameters as adopted in the experiment. It is found that the harmonic yield of O_2 in all the energy regions is much lower than that of Xe, which is qualitatively well consistent with the experimental data. In the following, we try to understand the underlying mechanism of the suppression of the below- and near-threshold harmonics in O_2.

First of all, we analyze the harmonic amplitude of trajectories in terms of the modified semiclassical method. According to Eq. (1), the harmonic amplitude of each trajectory contains two terms: the amplitude term a_j and the phase-dependent term $\exp(iS_q^j)$. In Fig. 4, we present the absolute values of $\exp(iS_q^j)$ and a_j as a function of the harmonic order for the two trajectories of O_2 and Xe, respectively. Note that the contribution of the second trajectory for the 15th harmonic is not presented, because its cutoff position is approximately at $q = 14$ harmonic [26]. Our simulation clearly shows that the values of $\exp(iS_q^j)$ of O_2 and its companion atom Xe are approximately the same for each trajectory. The reason is that the phase is closely relevant to the electron trajectory, which is less dependent on the atomic and molecular structures, especially for the electron with higher energy. On the other hand, the values of a_j for O_2 are much lower than those for Xe. Therefore, our analysis clearly shows that the suppression of harmonic yield for O_2 is mainly ascribed to the decrease of the amplitude a_j for O_2.

Second, we further reveal the underlying physics of the decrease of the amplitude a_j for O_2. According to Eq. (7), the amplitude of a_j is given by $a_j = d_{\rm ion}(\tilde{p}(t_{0j}))d^*_{\rm rec}(\tilde{p}(t_{rj}))$, where $d_{\rm ion}(\tilde{p}(t_{0j})) = \langle\tilde{p}(t_{0j})|H_{\rm int}(t_{0j})|\psi_0\rangle$ and $d_{\rm rec}(\tilde{p}(t_{rj})) = \langle\tilde{p}(t_{rj})|x|\psi_0\rangle$. Thus, the pronounced distinctions of the amplitude a_j between Xe and O_2 are ascribed to the different initial wave functions of Xe and O_2. After some algebra, we find that, for O_2, $d_{\rm ion}(\tilde{p}_j(t_{0j})) = -i[p_{0j} + A(t_{0j})]^2 \sin(p_{0j}\frac{R}{2}\cos\theta)\sum_\alpha C_\alpha\psi_\alpha(\tilde{p}(t_{0j}))$ and $d^*_{\rm rec}(\tilde{p}(t_{rj})) = -2\sin(p_{rj}\frac{R}{2}\cos\theta)\sum_\alpha C_\alpha\partial_{\tilde{p}}\psi_\alpha(\tilde{p}(t_{rj}))$ [50], where C_α is the coefficient extracted from the GAUSSIAN 09 quantum chemistry code [54], R is the internuclear distance, θ is the angle between the molecular axis and the laser polarization, and $\psi_\alpha(\tilde{p})$ is the atomic wave function in momentum space. In comparison with the Xe atom, there are two additional terms, $\sin(p_0\frac{R}{2}\cos\theta)$ in $d_{\rm ion}$ and $\sin(p_r\frac{R}{2}\cos\theta)$ in $d_{\rm rec}$, which are both from the two-center interference of the diatomic molecule of O_2 [50,51,59–61]. Next, we study the influence of the two-center interference terms [$\sin(p_0\frac{R}{2}\cos\theta)$ and $\sin(p_r\frac{R}{2}\cos\theta)$] and the atomic wave function $\psi_\alpha(\tilde{p})$ on the amplitude a_j, respectively.

In Figs. 5(a) and 5(b), we show the values of $|a_j|$ for O_2 with and without considering the two-center interference terms for the two trajectories, respectively. It clearly shows

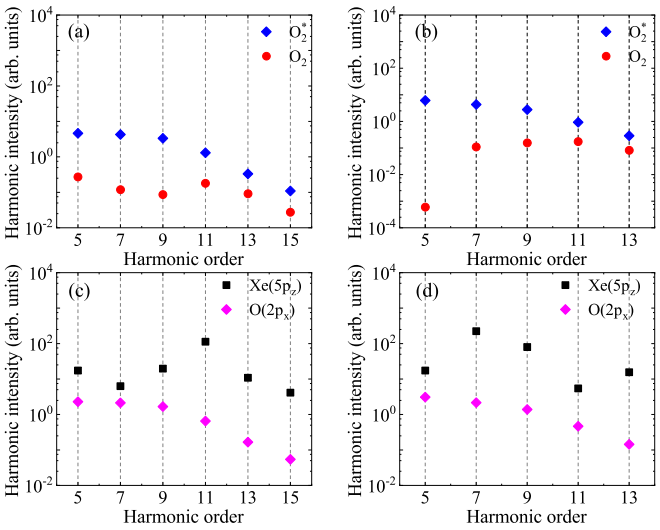

FIG. 5. The value of $|a_j|$ as a function of the harmonic order for O_2 with (blue diamond) and without (red dot) considering the two-center interference terms for (a) the first trajectory and (b) the second trajectory. The values of $|a_j|$ but without the two-center interference terms as a function of the harmonic order for the xenon atom with the orbital $5p_z$ and the oxygen atom with the orbital $2p_x$ for (c) the first trajectory and (d) the second trajectory.

that, after considering the sine terms, the value of $|a_j|$ decreases greatly for both trajectories, which is due to the small canonical momentums p_0 and p_r of the electron trajectories [50] and thus small values of two-center interference terms $\sin(p_0 \frac{R}{2} \cos\theta)$ and $\sin(p_j \frac{R}{2} \cos\theta)$. On the other hand, we present in Figs. 5(c) and 5(d) the values of $|a_j|$ but without the two-center interference terms for the Xe atom and the O atom with $j = 1$ and 2, respectively. It is found that this value for the oxygen atom also shows a significant suppression compared to the xenon atom for both trajectories. The possible reason is that the electron of the O atom in $2p$ orbital is bound tighter than that of the Xe atom in the $5p$ orbital, leading to the decrease of the tunneling ionization rate in the strong laser field. Similar results can be also found in Ref. [59]. Therefore, our results show that, due to the two-center interference effect and the tightly bounded orbital of the O atom, the below- and near-threshold harmonic yields of O_2 are greatly suppressed in comparison with Xe.

V. CONCLUSION

In conclusion, we have experimentally found a suppression of below- and near-threshold harmonic yields of O_2 compared to its companion atom Xe during the generation of an XUV comb. The experimental results can be well reproduced by a modified semiclassical method. Our analysis shows that the specific atomic or molecular structure, which is inherently included in the initial wave function of our theory, plays an essential role in the harmonic generation process. Moreover, we found that the two-center interference effect of the O_2 molecule, together with the tightly bounded orbital of the O atom, accounts for the suppression of below- and near-threshold harmonic yields of O_2 compared to its companion atom Xe. Our study provides useful information for the XUV-comb technique when extending the working media from atoms to complex systems.

ACKNOWLEDGMENTS

This work is supported by the National Key Research and Development Program of China (Grant No. 2019YFA0307702), the National Natural Science Foundation of China (Grants No. 11527807, No. 11834015, No. 11922413, and No. 11874392), the Strategic Priority Research Program of the Chinese Academy of Sciences (Grant No. XDB21010400), Science and Technology Department of Hubei Province (Grant No. 2020CFA029), and the K. C. Wong Education Foundation.

[1] For a recent review, see, e.g., I. Pupeza, C. K. Zhang, M. Högner, and J. Ye, Nat. Photonics **15**, 175 (2021), and reference therein.
[2] A. Cingöz, D. C. Yost, T. K. Allison, A. Ruehl, M. E. Fermann, I. Hartl, and J. Ye, Nature (London) **482**, 68 (2012).
[3] E. E. Eyler, D. E. Chieda, M. C. Stowe, M. J. Thorpe, T. R. Schibli, and J. Ye, Eur. Phys. J. D **48**, 43 (2008).
[4] S. D. Bergeson, A. Balakrishnan, K. G. H. Baldwin, T. B. Lucatorto, J. P. Marangos, T. J. McIlrath, T. R. O'Brian, S. L. Rolston, C. J. Sansonetti, J. Wen, N. Westbrook, C. H. Cheng, and E. E. Eyler, Phys. Rev. Lett. **80**, 3475 (1998).
[5] M. Haas, U. D. Jentschura, C. H. Keitel, N. Kolachevsky, M. Herrmann, P. Fendel, M. Fischer, T. Udem, R. Holzwarth, T. W. Hänsch, M. O. Scully, and G. S. Agarwal, Phys. Rev. A **73**, 052501 (2006).
[6] M. Herrmann, M. Haas, U. D. Jentschura, F. Kottmann, D. Leibfried, G. Saathoff, C. Gohle, A. Ozawa, V. Batteiger, S. Knunz, N. Kolachevsky, H. A. Schussler, T. W. Hänsch, and T. Udem, Phys. Rev. A **79**, 052505 (2009).
[7] M. H. Prior and H. A. Shugart, Phys. Rev. Lett. **27**, 902 (1971).
[8] J. C. Berengut and V. V. Flambaum, Nucl. Phys. News **20**, 19 (2010).
[9] C. J. Campbell, A. G. Radnaev, A. Kuzmich, V. A. Dzuba, V. V. Flambaum, and A. Derevianko, Phys. Rev. Lett. **108**, 120802 (2012).
[10] B. Seiferle, L. von der Wense, P. V. Bilous, I. Amersdorffer, C. Lemell, F. Libisch, S. Stellmer, T. Schumm, C. E. Düllmann, A. Pálffy, and P. G. Thirolf, Nature (London) **573**, 243 (2019).
[11] L. von der Wense, B. Seiferle, M. Laatiaoui, J. B. Neumayr, H.-J. Maier, H.-F. Wirth, C. Mokry, J. Runke, K. Eberhardt, C. E. Düllmann, N. G. Trautmann, and P. G. Thirolf, Nature (London) **533**, 47 (2016).
[12] A. K. Mills, T. J. Hammond, M. H. C. Lam, and D. J. Jones, J. Phys. B: At., Mol. Opt. Phys. **45**, 142001 (2012).
[13] C. Benko, L. Q. Hua, T. K. Allison, F. Labaye, and J. Ye, Phys. Rev. Lett. **114**, 153001 (2015).
[14] M. X. Na, A. K. Mills, F. Boschini, M. Michiardi, B. Nosarzewski, R. P. Day, E. Razzoli, A. Sheyerman, M.

Schneider, G. Levy, S. Zhdanovich, T. P. Devereaux, A. F. Kemper, D. J. Jones, and A. Damascelli, Science **366**, 1231 (2019).
[15] T. Saule, S. Heinrich, J. Schötz, N. Lilienfein, M. Högner, O. deVries, M. Plötner, J. Weitenberg, D. Esser, J. Schulte, P. Russbueldt, J. Limpert, M. F. Kling, U. Kleineberg, and I. Pupeza, Nat. Commun. **10**, 458 (2019).
[16] R. J. Jones, K. D. Moll, M. J. Thorpe, and J. Ye, Phys. Rev. Lett. **94**, 193201 (2005).
[17] C. Gohle, T. Udem, M. Herrmann, J. Rauschenberger, R. Holzwarth, H. A. Schuessler, F. Krausz, and T. W. Hänsch, Nature (London) **436**, 234 (2005).
[18] C. K Zhang, S. B. Schoun, C. M. Heyl, G. Porat, M. B. Gaarde, and J. Ye, Phys. Rev. Lett. **125**, 093902 (2020).
[19] J. Nauta, J.-H. Oelmann, A. Borodin, A. Ackermann, P. Knauer, I. S. Muhammad, R. Pappenberger, T. Pfeifer, and J. R. Crespo López-Urrutia, Opt. Express **29**, 2624 (2021).
[20] A. L'huillier, K. J. Schafer, and K. C. Kulander, J. Phys. B: At., Mol. Opt. Phys. **24**, 3315 (1991).
[21] W. H. Xiong, L. Y. Peng, and Q. H. Gong, J. Phys. B: At., Mol. Opt. Phys. **50**, 032001 (2017).
[22] P. B. Corkum, Phys. Rev. Lett. **71**, 1994 (1993).
[23] K. J. Schafer, B. Yang, L. F. DiMauro, and K. C. Kulander, Phys. Rev. Lett. **70**, 1599 (1993).
[24] D. C. Yost, T. R. Schibli, J. Ye, J. L. Tate, J. Hostetter, M. B. Gaarde, and K. J. Schafer, Nat. Phys. **5**, 815 (2009).
[25] H. Soifer, P. Botheron, D. Shafir, A. Diner, O. Raz, B. D. Bruner, Y. Mairesse, B. Pons, and N. Dudovich, Phys. Rev. Lett. **105**, 143904 (2010).
[26] J. A. Hostetter, J. L. Tate, K. J. Schafer, and M. B. Gaarde, Phys. Rev. A **82**, 023401 (2010).
[27] M. Th. Hassan, T. T. Luu, A. Moulet, O. Raskazovskaya, P. Zhokhov, M. Garg, N. Karpowicz, A. M. Zheltikov, V. Pervak, F. Krausz, and E. Goulielmakis, Nature (London) **530**, 66 (2016).
[28] P. C. Li, Y. L. Sheu, C. Laughlin, and Shih-I Chu, Phys. Rev. A **90**, 041401(R) (2014).
[29] P. C. Li, Y. L. Sheu, C. Laughlin, and Shih I. Chu, Nat. Commun. **6**, 7178 (2015).
[30] G. Porat, C. M. Heyl, S. B. Schoun, C. Benko, N. Dörre, K. L. Corwin, and J. Ye, Nat. Photonics **12**, 387 (2018).
[31] J. Zhang, L. Q. Hua, Z. Chen, M. F. Zhu, C. Gong, and X. J. Liu, Chin. Phys. Lett. **37**, 124203 (2020).
[32] E. Frumker, C. T. Hebeisen, N. Kajumba, J. B. Bertrand, H. J. Wörner, M. Spanner, D. M. Villeneuve, A. Naumov, and P. B. Corkum, Phys. Rev. Lett. **109**, 113901 (2012).
[33] J. Itatani, J. Levesque, D. Zeidler, H. Niikura, H. Pépin, J. C. Kieffer, P. B. Corkum, and D. M. Villeneuve, Nature (London) **432**, 867 (2004).
[34] M. Lein, N. Hay, R. Velotta, J. P. Marangos, and P. L. Knight, Phys. Rev. Lett. **88**, 183903 (2002).
[35] B. B. Augstein, and C. Figueira de Morisson Faria, Mod. Phys. Lett. B **26**, 1130002 (2012).
[36] E. Frumker, N. Kajumba, J. B. Bertrand, H. J. Wörner, C. T. Hebeisen, P. Hockett, M. Spanner, S. Patchkovskii, G. G. Paulus, D. M. Villeneuve, A. Naumov, and P. B. Corkum, Phys. Rev. Lett. **109**, 233904 (2012).
[37] S. Haessler, J. Caillat, and P. Salières, J. Phys. B: At., Mol. Opt. Phys. **44**, 203001 (2011).
[38] H. Yun, S. J. Yun, G. H. Lee, and C. H. Nam, J. Phys. B: At., Mol. Opt. Phys. **50**, 022001 (2017).
[39] L. Rego, C. Hernández-García, A. Picón, and L. Plaja, New J. Phys. **22**, 043012 (2020).
[40] C. Vozzi, F. Calegari, E. Benedetti, J.-P. Caumes, G. Sansone, S. Stagira, M. Nisoli, R. Torres, E. Heesel, N. Kajumba, J. P. Marangos, C. Altucci, and R. Velotta, Phys. Rev. Lett. **95**, 153902 (2005).
[41] C. Vozzi, F. Calegari, E. Benedetti, R. Berlasso, G. Sansone, S. Stagira, M. Nisoli, C. Altucci, R. Velotta, R. Torres, E. Heesel, N. Kajumba, and J. P. Marango, J. Phys. B: At., Mol. Opt. Phys. **39**, S457 (2006).
[42] R. Torres, T. Siegel, L. Brugnera, I. Procino, Jonathan G. Underwood, C. Altucci, R. Velotta, E. Springate, C. Froud, I. C. E. Turcu, S. Patchkovskii, M. Yu. Ivanov, O. Smirnova, and J. P. Marangos, Phys. Rev. A **81**, 051802(R) (2010).
[43] J. Zhang, L. Q. Hua, S. G. Yu, Z. Chen, and X. J. Liu, Chin. Phys. B **28**, 044206 (2019).
[44] J. Zhang, L. Q. Hua, S. G. Yu, Y. L. Wang, M. F. Zhu, Z. R. Xiao, C. Gong, and X. J. Liu, Phys. Rev. A **103**, 032822 (2021).
[45] M. Lewenstein, Ph. Balcou, M. Yu. Ivanov, Anne L'Huillier, and P. B. Corkum, Phys. Rev. A **49**, 2117 (1994).
[46] P. Salières, B. Carré, L. Le Déroff, F. Grasbon, G. G. Paulus, H. Walther, R. Kopold, W. Becker, D. B. Milošević, A. Sanpera, and M. Lewenstein, Science **292**, 902 (2001).
[47] M. M. Liu, M. Han, P. P. Ge, C. X. He, Q. H. Gong, and Y. Q. Liu, Phys. Rev. A **97**, 063416 (2018).
[48] E. Priori, G. Cerullo, M. Nisoli, S. Stagira, S. De Silvestri, P. Villoresi, L. Poletto, P. Ceccherini, C. Altucci, R. Bruzzese, and C. de Lisio, Phys. Rev. A **61**, 063801 (2000).
[49] R. Kopold, W. Becker, and M. Kleber, Opt. Commun. **179**, 39 (2000).
[50] C. Figueira de Morisson Faria, Phys. Rev. A **76**, 043407 (2007).
[51] X. Y. Lai and C. Figueira de Morisson Faria, Phys. Rev. A **88**, 013406 (2013).
[52] C. B. Madsen and L. B. Madsen, Phys. Rev. A **74**, 023403 (2006).
[53] C. Altucci, R. Velotta, J. P. Marangos, E. Heesel, E. Springate, M. Pascolini, L. Poletto, P. Villoresi, C. Vozzi, G. Sansone, M. Anscombe, J-P. Caumes, S. Stagira, and M. Nisoli, Phys. Rev. A **71**, 013409 (2005).
[54] M. J. Frisch, G. W. Trucks, H. B. Schlegel *et al.*, GAUSSIAN 09 (Revision D.01) (Gaussian, Inc., Wallingford, CT, 2013).
[55] T. K. Allison, A. Cingöz, D. C. Yost, and J. Ye, Phys. Rev. Lett. **107**, 183903 (2011).
[56] B. Shan, X. M. Tong, Z. X. Zhao, Z. H. Chang, and C. D. Lin, Phys. Rev. A **66**, 061401(R) (2002).
[57] G. H. Li, J. P. Yao, H. S. Zhang, C. R. Jing, B. Zeng, W. Chu, J. L. Ni, H. Q. Xie, X. J. Liu, J. Chen, Y. Cheng, and Z. Z. Xu, Phys. Rev. A **88**, 043401 (2013).
[58] X. M. Tong, Z. X. Zhao, and C. D. Lin, Phys. Rev. A **66**, 033402 (2002).
[59] Z. Y. Lin, X. Y. Jia, C. L. Wang, Z. L. Hu, H. P. Kang, W. Quan, X. Y. Lai, X. J. Liu, J. Chen, B. Zeng, W. Chu, J. P. Yao, Y. Cheng, and Z. Z. Xu, Phys. Rev. Lett. **108**, 223001 (2012).
[60] Z. L. Hu, X. Y. Lai, X. J. Liu, and J. Chen, Phys. Rev. A **89**, 043401 (2014).
[61] R. P. Sun, X. Y. Lai, S. G. Yu, Y. L. Wang, S. P. Xu, W. Quan, and X. J. Liu, Phys. Rev. Lett. **122**, 193202 (2019).